Diagnostics of AC Transmission Line Insulators using an FBG-Based E-Field Sensor

Veeresh Ramnarine[1], Vidyadhar Peesapati[1], Siniša Djurović[1], Ramy Afia[1], Christopher Land[2]
[1]*The University of Manchester, Manchester, United Kingdom*
[2]*National Grid, London, United Kingdom*

***Abstract*—As the number of ageing transmission line insulators in electrical grids increases, novel means for determining the health of these assets are required. This work presents a 3D electric field sensor using fibre Bragg grating (FBG) technology for condition monitoring of composite insulators. Four 400 kV insulator samples: one healthy and three with various internal defects were energised in a high voltage laboratory and the generated electric fields were measured using the sensor. The obtained profiles of electric field along insulators with defects were distorted compared to the profile of the healthy insulator. Defects as short as 2" at the live end yielded measurable distortions. The results show that the proposed FBG electric field sensor can provide early signs of degradation and has potential to help reduce unplanned outages arising from insulator failures, improving grid reliability.**

***Index Terms*—condition monitoring, insulator testing, electric fields, optical fiber sensors**

I. Introduction

Overhead line insulators are critical components of transmission infrastructure as it supports the high voltage (HV) conductors on the network as well as provide insulation to the towers [1]. Insulators are classified based on the type of insulation material used: ceramic or polymeric [2]. Polymeric insulators, also known as composite insulators, comprise a fibre reinforced plastic (FRP) core rod which provides mechanical strength and polymer housing which ensures sufficient leakage distance [3]. Due to the use of these materials, composite insulators have several advantages over ceramic insulators such as lighter in weight and higher voltage flashover ratings especially in polluted conditions [4]. However, transmission line insulators which operate in outdoor environments are subjected to increased environmental stresses due to climate change effects [5] and electric stresses as a result of higher harmonics from interconnections of inverter-based resources [6]. These ageing factors can result in conductive defects between the rod and polymeric housing which lead to partial discharges and increased temperature, promoting further stresses [7]. Such defects, if undetected, can cause fracture of the insulator and consequently line outages. Thus, in order to maintain a reliable grid, condition monitoring of these insulators is required. Several techniques of online monitoring for insulator exist including: infrared thermography, ultraviolet detection and electric field measurement [8]. Electric field measurement is effective since internal defects in the composite insulators would produce a permanent distortion in the surrounding electric field. Thus, this method has been applied to diagnostics of insulators in electrical grids since the 1990s when a capacitive space potential probe was developed for such application [9]. Electro-optic probes have also been demonstrated potential for electric field monitoring of composite insulators, based on small scale lab tests in [10], but these types of sensors are typically more costly. Fibre Bragg grating (FBG) sensing is another promising technology that can be used for electric field measurements around HV assets [11]. In [12], an orthogonal assembly of three FBG based electric field probes was used to measure the electric field along 66 kV composite insulator. The measurements closely matched the theoretical electric field obtained from simulations, indicating the effectiveness of the sensor for this application. The sensor also has features of relatively small footprint (sensing section less than 10mm^3), only dielectric materials and power passivity, which are advantageous for use in live line measurements especially near the HV end of the insulator. This paper therefore applies the FBG electric field sensor to 400 kV composite insulator samples with and without internal defects to determine whether the sensor can be used for diagnostics of AC transmission line insulators.

II. Overview of the FBG Electric Field Sensor

A fibre Bragg grating sensor comprises a single mode fibre with periodic changes in the refractive index of the core, known as 'gratings' [13]. These gratings typically range from 1mm to 10mm. When the fibre is illuminated with broadband light, the gratings reflect a narrow spectrum of light back to the source, centred at a specific wavelength, termed Bragg wavelength (λ_B). The Bragg wavelength is inherently affected by temperature and strain and thus FBG sensors can be used for monitoring these parameters by correlating to changes in λ_B [14]. Fig. 1 illustrates the schematic of a typical FBG sensor and the principle of operation.

FBG sensors can indirectly measure other parameters by pairing with strain transducers. In the case of electric field sensing, piezoelectric materials are suitable strain traducers due to the converse piezoelectric effect [15]. The FBG electric field sensor used in this study includes three substrates of piezoelectric material, PMN-PT, each with dimensions 5mm x 2mm x 0.5mm bonded to the gratings of three FBG sensors. Fig. 2 shows one of the three FBG sensor/piezoelectric pairings. These pairings were orthogonally assembled using a PTFE frame, as shown in Fig. 3, which enables measurements

979-8-3315-8138-1

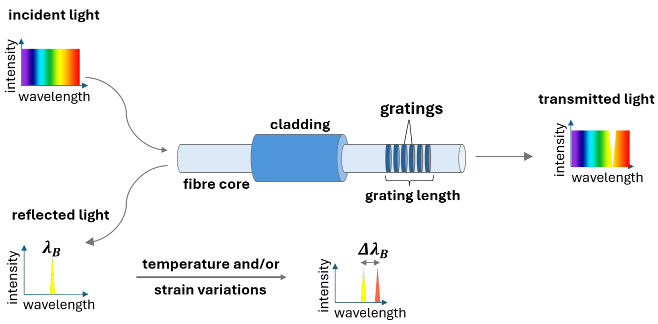

Fig. 1. Principle of operation of FBG sensors.

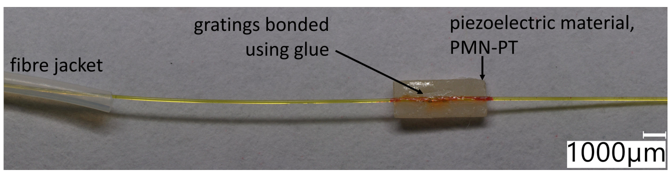

Fig. 2. FBG sensor/piezoelectric paring for assembling electric field sensor.

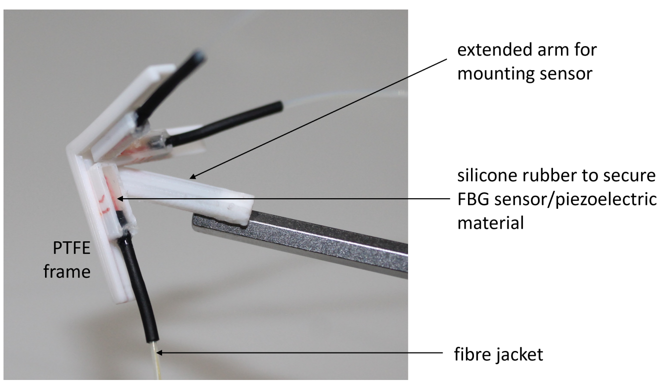

Fig. 3. FBG electric field sensor.

of the electric field components in the X, Y, Z axes: E_x, E_y, E_z.

When the sensor is exposed to an AC electric field, the strain generated in the piezoelectric materials and hence the Bragg wavelengths, λ_B, of each FBG sensor would oscillate at the power frequency. The magnitudes of these oscillations: can be expressed in terms of the electric field components using the following general form:

$$\Delta\lambda_{B_1} = a_1 E_x + b_1 E_y + c_1 E_z \tag{1}$$

$$\Delta\lambda_{B_2} = a_2 E_x + b_2 E_y + c_3 E_z \tag{2}$$

$$\Delta\lambda_{B_3} = a_3 E_x + b_2 E_y + c_3 E_z \tag{3}$$

where $\Delta\lambda_{B_1}$, $\Delta\lambda_{B_2}$, $\Delta\lambda_{B_3}$ are the Bragg wavelength oscillations for each of the three FBG sensors in the orthogonal assembly. The coefficients in the above general equations can be determined from empirical tests in known electric fields. Once fully defined, measurement of the Bragg wavelengths can be used to compute the electric field. For this sensor, the coefficients were previously determined, and the corresponding equations were stated in [12]. The magnitude of the electric field, $|E|$, can then be calculated by:

$$|E| = \sqrt{E_x^2 + E_y^2 + E_z^2} \tag{4}$$

In practice, the Bragg wavelength oscillations are measured using an optical interrogator. This device transmits the broadband light to the FBG sensors, receives the reflected lights and interprets the Bragg wavelength. When sampled at a sufficiently high rate, oscillations due to the AC electric field can be measured. This process has the convenient advantage of separating Bragg wavelength changes due to temperature as this would typically be slower than 50/60Hz.

III. Insulator Test Samples

For this study, 400 kV suspension type composite insulator samples were provided by National Grid UK. The silicone rubber housing was 108” wide and included 79 sheds: 27 sheds of larger diameter (outer sheds) and 52 sheds of smaller diameter (inner sheds) arranged in pairs. Four samples were used for testing: one healthy insulator and three insulators with purposely built internal defects. The internal defects in each defective sample varied in length and position, as shown in red in Fig. 4.

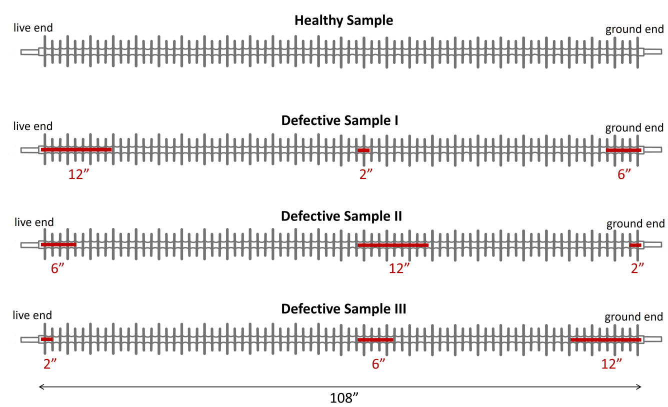

Fig. 4. Composite insulator samples for testing (conductive defects shown in red).

IV. Test Set Up

A. FBG Interrogator

The Bragg wavelengths of each FBG sensor in the orthogonal assembly were measured using a commercially available interrogator, SmartScan from SmartFibres Ltd. This device is equipped with four channels enabling simultaneous measurements from the three sensors. The Bragg wavelengths were recorded on a PC connected to the interrogator via Ethernet for computing of the Bragg wavelength oscillations: $\Delta\lambda_{B_1}$, $\Delta\lambda_{B_2}$, $\Delta\lambda_{B_3}$ and hence the electric field components: E_x, E_y, E_z.

979-8-3315-8138-1

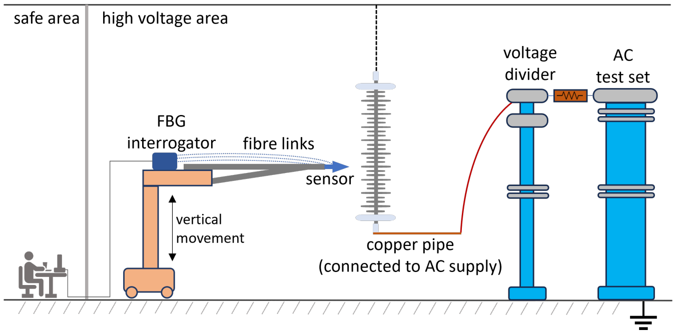

Fig. 5. Schematic of test set up in high voltage laboratory.

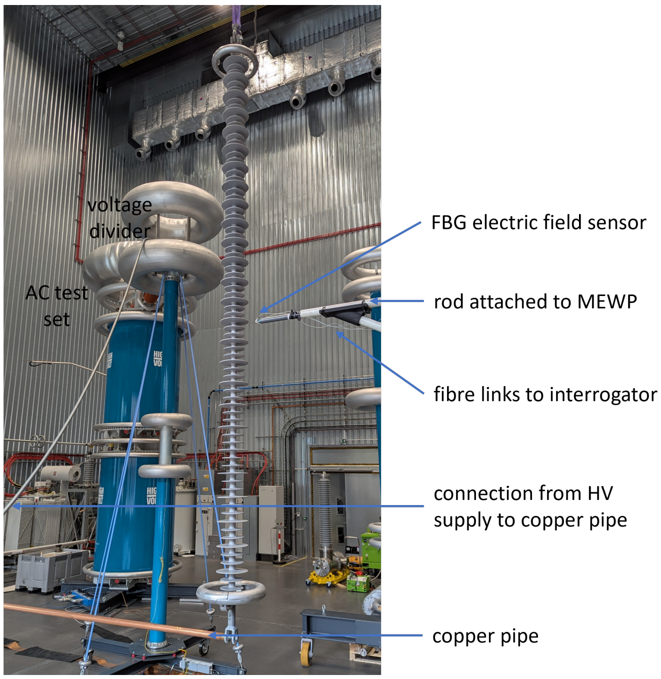

Fig. 6. Insulator testing in HV laboratory.

B. High Voltage Test Circuit

Each insulator was individually tested in a laboratory equipped with an 800 kV AC test set (by High Volt) and a voltage divider for sampling the output voltage. The circuit was set up by suspending the insulator from the ground end using an overhead chain block. The live end was approximately 2m above the floor and connected to the AC supply using a copper pipe. The FBG electric field sensor was attached to the end of a 3m length fibre glass rod which was fixed on a mobile elevated work platform (MEWP). The MEWP was set up with remote control so that the platform and hence the sensor can be moved along the insulator sheds when energised. The test set up is shown in Fig. 5 and Fig. 6.

For each insulator, 150 kVrms at 50 Hz was used as the test voltage which is 35% lower than the rated voltage of $400/\sqrt{3}$ kV. This voltage was selected to reduce the stress on the insulators which are particularly susceptible to degradation due to the internal defects. The electric field profiles would

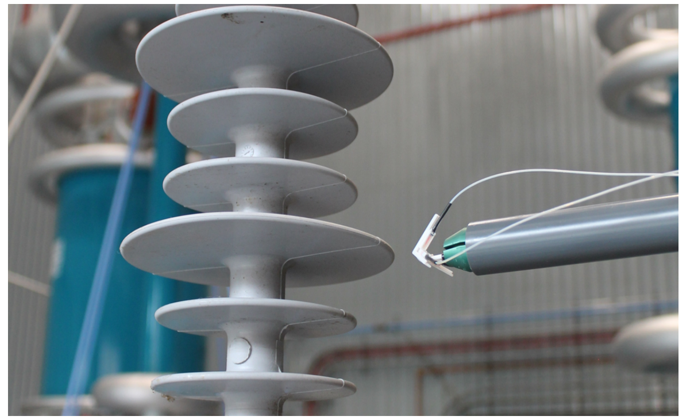

Fig. 7. FBG electric field sensor at edge of composite insulator shed during testing.

be similar at the lower voltage but scaled down by 35% and therefore the objective of the test which was to measure distortions due to the defects would not be affected.

C. Measurement Points

For each test, the sensor was set up 25mm away from the edges of the outer sheds. Starting at the live end, the sensor was moved to each outer shed and between the pairs of inner sheds for recording the Bragg wavelengths. Due to the corona rings, some sheds near the ends were not included. The positions of the measurement points, relative to the insulator is shown in the cross section in Fig. 8. Since the MEWP was remotely controlled in the safe area located away from the insulator, the actual measurement position would vary by a few millimetres above or below the specified measurement point. The Cartesian axes of the sensor is also included in Fig. 8, indicating that the X component of the electric field was radial while the Z component was axial to the insulator.

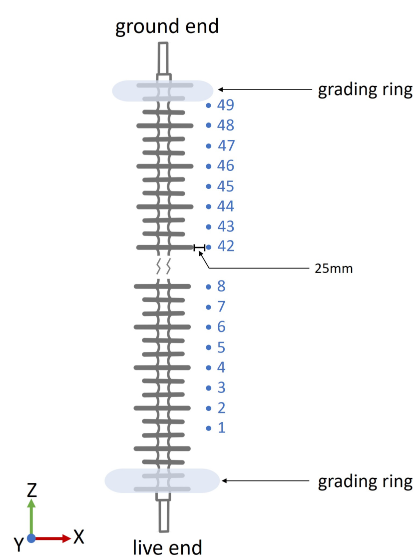

Fig. 8. Schematic of insulator showing locations of measurement points.

V. Results

For each insulator, the Bragg wavelengths at the 49 measurement points were recorded and then used to compute the electric field components in the X, Y, Z axes: E_x, E_y, E_z and magnitude, $|E|$. The Y component, which is tangential to the insulator sheds, was the lowest among the three and not used in this analysis. The electric field magnitude along the healthy insulator followed an uneven 'U' shaped profile with the field at HV end being higher than at the ground end, which is typical of overhead line insulators [16]. The X and Z components for the healthy insulator exhibited similar profiles. These measurements form a baseline for comparison with profiles of other insulators. Any distortions relative to the baseline would therefore indicate the presence of defects.

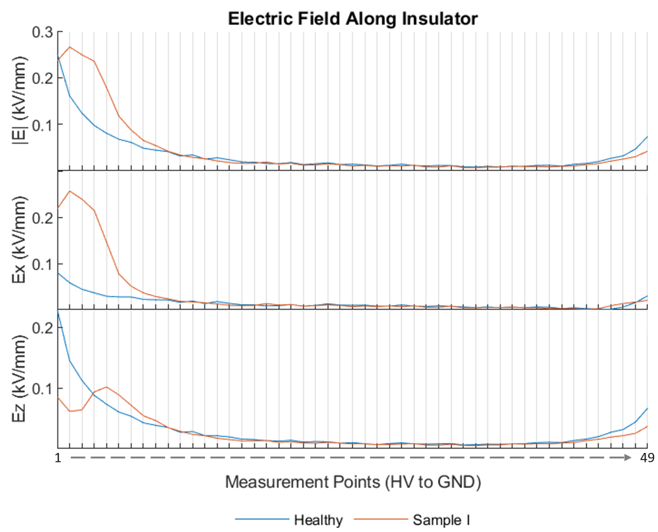

Fig. 9. Electric field profiles - defective sample I vs healthy sample .

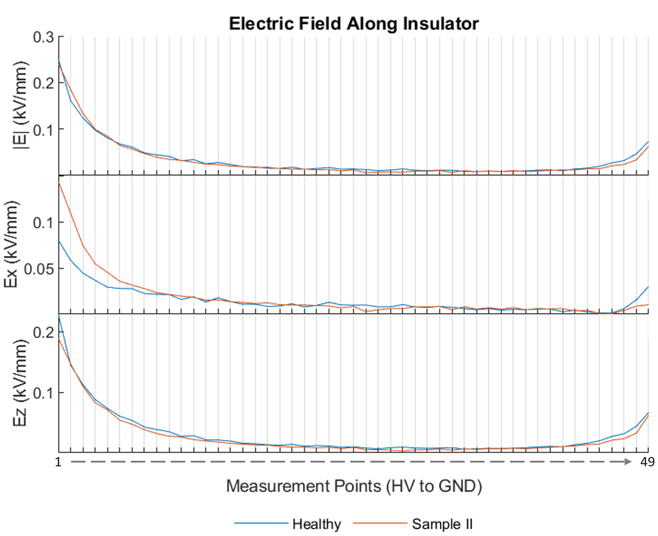

Fig. 10. Electric field profiles - defective sample II vs healthy sample .

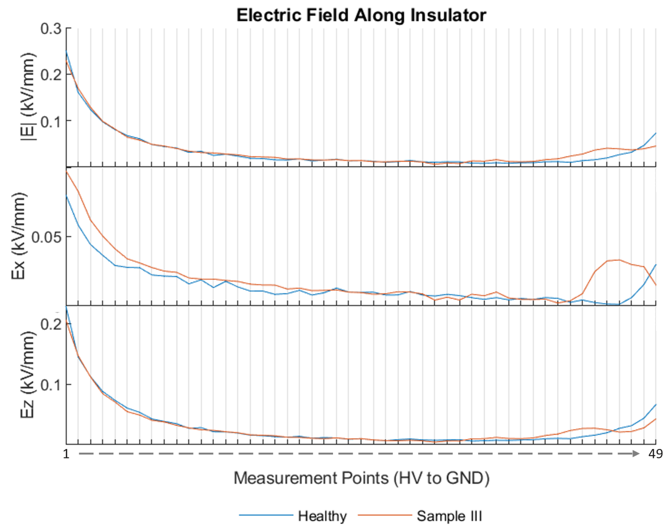

Fig. 11. Electric field profiles - defective sample II vs healthy sample .

The electric field profiles for defective samples I, II and III are plotted in Fig. 9, Fig. 10 and Fig. 11 along with the healthy profiles for reference. All profiles for sample I included significant distortion near the HV end due to the 12" defect at that location. Deviations from the baseline near the ground end (approaching measurement point 49) also occurred as a result of the 6" defect. The electric field profiles for sample II more closely matched the healthy profiles since the defects at the ends (where the electric field sharply increases) were shorter. The electric field magnitude, $|E|$, and Z axis component, E_z, near the HV end were similar in magnitude to the healthy sample, despite the presence of the 6" defect. This was due to the starting point of the measurement which was just above the end of the defect location. However, the X axis component, E_x, showed deviations of up to 87% between measurement points 1-6. This case highlights that some defects may not be detectable by using only the electric field magnitude, and that measuring the components is useful for diagnostics. The measurements for sample III, which had a 2" defect near the HV end, also yielded an increase in E_x of up to 42% between measurement points 1-6 while $|E|$ and E_z showed no significant change. This sample was also fitted with a 12" defect at the ground end and due to the length, distortions occurred in all the plots.

For all the samples, the profiles at the middle of the insulator were of similar shape even with defects up to 12". The electric field in this region of the insulator was lower than the ends, dropping below 0.001 kV/mm for some points. Distortions at this magnitude would therefore be difficult to measure, especially with variability in measurement due to positioning of the insulators and sensor, along with instrumentation uncertainty in the FBG interrogator. The results, however, show that defects at the ends, especially near the HV fitting, were easily identified. This is the likely case for composite insulators in service as the electric field is highest at the live end, triggering

979-8-3315-8138-1

partial discharge and creation of conductive carbonized traces [17]. A review of composite insulator failures in [18] showed that the fracture of the core rod due to internal degradation occurred near the HV end, between the 3rd and 8th shed. Additionally, as the length of the defect increased from 2” to 12” (2% to 11% of the overall insulator length), the distortions were larger and clearly showed the presence of a defect. The critical defect length (maximum length for safe operation) is dependent on the overall power system and estimated overvoltages but typically may be longer than the lengths in this study. For example, in the Italian grid, the critical length for defects near the HV end was estimated to be 25% of the insulator [19]. Based on the trends observed in Fig. 9, Fig. 10 and Fig. 11, the FBG electric field sensor can identify the presence of defects smaller than the 25% threshold and hence provide early warning of failure.

VI. Conclusion

In this paper, a novel electric field sensor, based on fibre Bragg grating (FBG) technology, is proposed for cdiagnostics of AC transmission line insulators. The sensor is immune to electromagnetic interference, power passive, made of only dielectric materials and has a relatively small footprint (less than 10mm^3), and therefore can be used in high voltage areas regions with low risk. The performance of the sensor for this application was tested using four 400 kV composite insulator samples energised in a high voltage laboratory. The tests involved moving the sensor along the insulators and measuring the 3D electric field vector at the ends of the insulator sheds. The results show the profiles of electric field magnitude were distorted in samples that included 12” defects (11% of the insulator length) at the live or grounded ends. For insulators with shorter defects at the ends, the electric field magnitude did not yield significant deviations when compared to the profile along the healthy insulator. For example, the maximum relative change in electric field magnitude was 15% for a 6” defect located at the live end. However, the X axis component of the electric field produced a relative change up to 86% due to the 6” defect. Thus, the ability to extract the electric field components from the sensor is a useful feature and enables early detection of faults on composite insulators. The outcome of this work demonstrates that the proposed FBG electric field sensor is effective for condition monitoring of transmission line insulators, which can help prevent failures and unplanned grid outages.

Acknowledgment

The authors would like to thank National Grid UK for supporting this research.

References

[1] C. R. Bayliss and B. J. Hardy, eds., *Insulators*, pp. 163–180. Oxford: Newnes, 2007.

[2] K. Sit, A. K. Pradhan, B. Chatterjee, and S. Dalai, “A review on characteristics and assessment techniques of high voltage silicone rubber insulator,” *IEEE Transactions on Dielectrics and Electrical Insulation*, vol. 29, no. 5, pp. 1889–1903, 2022.

[3] V. E. Ogbonna, P. I. Popoola, O. M. Popoola, and S. O. Adeosun, “A comparative study on the failure analysis of field failed high voltage composite insulator core rods and recommendation of composite insulators: A review,” *Engineering Failure Analysis*, vol. 138, p. 106369, 2022.

[4] A. Tzimas, E. D. Silva, S. M. Rowland, B. Boumecid, M. Queen, and M. Michel, “Asset management frameworks for outdoor composite insulators,” *IEEE Transactions on Dielectrics and Electrical Insulation*, vol. 19, no. 6, pp. 2044–2054, 2012.

[5] V. Y. Ushakov, A. V. Mytnikov, and I. U. Rakhmonov, *Effects on Equipment Causing Insulation Aging and Failure*, pp. 117–127. Cham: Springer Nature Switzerland, 2023.

[6] G. C. Montanari, R. Hebner, P. Morshuis, and P. Seri, “An approach to insulation condition monitoring and life assessment in emerging electrical environments,” *IEEE Transactions on Power Delivery*, vol. 34, no. 4, pp. 1357–1364, 2019.

[7] B. Lutz, L. Cheng, Z. Guan, L. Wang, and F. Zhang, “Analysis of a fractured 500 kV composite insulator - identification of aging mechanisms and their causes,” *IEEE Transactions on Dielectrics and Electrical Insulation*, vol. 19, no. 5, pp. 1723–1731, 2012.

[8] report, CIGRE TB 545 (WG B2.21), Assessment of in-service Composite Insulators by using Diagnostic Tools, August 2013.

[9] G. H. Vaillancourt, S. Carignan, and C. Jean, “Experience with the detection of faulty composite insulators on high-voltage power lines by the electric field measurement method,” *IEEE Transactions on Power Delivery*, vol. 13, no. 2, pp. 661–666, 1998.

[10] C. Volat, M. Jabbari, M. Farzaneh, and L. Duvillaret, “New method for in live-line detection of small defects in composite insulator based on electro-optic E-field sensor,” *IEEE Transactions on Dielectrics and Electrical Insulation*, vol. 20, no. 1, pp. 194–201, 2013.

[11] V. Ramnarine, V. Peesapati, and S. Djurović, “Electrodeless piezoelectric based sensor for electric field measurement in high voltage applications,” *IEEE Transactions on Instrumentation and Measurement*, 2025. To be published.

[12] V. Ramnarine, V. Peesapati, S. Djurović, F. Liu, R. Afia, J. Knapper, and R. Raj, “FBG sensor assembly for 3D electric field measurement along composite insulators,” in *2025 IEEE Conference on Electrical Insulation and Dielectric Phenomena (CEIDP)*, pp. 925–928, 2025.

[13] K. O. Hill and G. Meltz, “Fiber Bragg grating technology fundamentals and overview,” *Journal of Lightwave Technology*, vol. 15, no. 8, pp. 1263–1276, 1997.

[14] W. W. Morey, G. Meltz, and W. H. Glenn, “Fiber optic Bragg grating sensors,” in *Proc.SPIE*, vol. 1169, pp. 98–107, 1990.

[15] A. Ballato, “Piezoelectricity: old effect, new thrusts,” *IEEE Transactions on Ultrasonics, Ferroelectrics, and Frequency Control*, vol. 42, no. 5, pp. 916–926, 1995.

[16] M. R. Halloum and B. S. Reddy, “Investigations on the failure of in-service 400-kV composite insulator,” *IEEE Transactions on Dielectrics and Electrical Insulation*, vol. 30, no. 6, pp. 2769–2778, 2023.

[17] G. Pang, Z. Zhang, J. Li, S. Q. Li, and S. M. Rowland, “Effects of AC corona discharge on GFRP core rods used in composite insulators,” *IEEE Transactions on Dielectrics and Electrical Insulation*, vol. 32, no. 4, pp. 2375–2384, 2025.

[18] J. Wang, X. Liang, and Y. Gao, “Failure analysis of decay-like fracture of composite insulator,” *IEEE Transactions on Dielectrics and Electrical Insulation*, vol. 21, no. 6, pp. 2503–2511, 2014.

[19] M. d. Nigris, I. Gutman, and A. Pigini, “Live-line maintenance of AC overhead lines equipped with non ceramic insulators (NCI),” in *IEEE PES T&D 2010*, pp. 1–6, 2010.

979-8-3315-8138-1